Toughness improvement and anisotropy in semicrystalline physical hydrogels

Check for updates

Cigdem Bilici[a], Damla Karaarslan[b], Semra Ide[b], Oguz Okay[a,*]

[a] Department of Chemistry, Istanbul Technical University, 34469, Maslak, Istanbul, Turkey
[b] Departments of Physics Engineering and Nanotechnology & Nanomedicine, Hacettepe University, 06800, Beytepe, Ankara, Turkey

HIGHLIGHTS

- High-strength physical hydrogels with anisotropic properties are prepared.
- Directional toughness improvement is achieved in semicrystalline hydrogels.
- Young's modulus of the hydrogel is 161 and 76 MPa along different directions.

ABSTRACT

A major challenge in the gel science is to create mechanically strong hydrogels with anisotropic properties as observed in many biological tissues. Here, we report a simple one-step method of producing high-strength physical hydrogels exhibiting microstructural and mechanical anisotropy. As the precursor material, we use semicrystalline shape-memory hydrogels consisting of poly(N, N-dimethylacrylamide) chains interconnected by n-octadecyl acrylate (C18A) segments forming crystalline domains and hydrophobic associations acting as switching segments and netpoints, respectively. To generate anisotropic microstructure, we impose a pre-stretching on the isotropic hydrogel sample above the melting temperature T_m of its crystalline domains followed by cooling below T_m under strain to fix the elongated shape of the gel sample. A significant microstructural and mechanical anisotropy was achieved that could be tuned by the magnitude of the prestretch ratio λ_o. Directional brittle-to-ductile and ductile-to-brittle transitions could be induced by adjusting the prestretch ratio λ_o. Small- and wide-angle X-ray scattering measurements and mechanical tests highlight a critical prestretch ratio λ_o at which the hydrogel exhibits the highest microstructural and mechanical anisotropy due to the finite extensibility of the network chains. At $\lambda_o = 1.8$, the hydrogel exhibits Young's moduli of 161 ± 14 and 76 ± 7 MPa, and toughness of 16 ± 1 and 1.3 ± 0.1 MJ m^{-3} along and perpendicular to the prestretching direction, respectively.

1. Introduction

Owing to their similarities to biological tissues, hydrogels as soft and smart materials have important functions in a variety of biological and biomedical applications [1]. Although hydrogels are traditionally brittle and exhibit a low modulus of elasticity in the range of kPa, significant progress has been achieved in the past 15 years in the design of mechanically strong and tough hydrogels [2]. Several techniques developed so far enable preparation of hydrogels with mechanical performances approaching to those of biological systems.

Another challenge to be addressed in the gel science is to create mechanically strong hydrogels with anisotropic properties, as observed in many biological tissues such as skin, muscle, and articular cartilage possessing anisotropically oriented hierarchical structures [3]. To achieve this goal, nanofillers such as nanofibers [4,5], graphene oxide [6], nanosheets [7], nanotubes [8], or nanodisks [9,10] in a precursor dispersion were first oriented and then the oriented microstructure was fixed by gelation. Anisotropic hydrogels were also produced by directional freezing [11–13], or by orienting the network chains of isotropic hydrogels under an external force followed by fixing the anisotropic structure via in situ polymerization [14–18]. Kajiyama et al. reported stress-induced orientation of lamellar crystals in covalently cross-linked semicrystalline hydrogels [19]. Although not reported, these hydrogels should exhibit anisotropic mechanical properties. Such hydrogels were

* Corresponding author.
  E-mail address: okayo@itu.edu.tr (O. Okay).

also prepared via a two-step procedure consisting of prestretching the network chains of isotropic hydrogels to a certain strain and subsequent fixation of the stretched chain conformation by ionic cross-linking [15,16]. Another technique to create anisotropy in hydrogels is ion-diffusion-induced orientation and cross-linking of semi-rigid polyelectrolytes followed by double-networking with an amorphous second network [20–23]. Gong et al. recently showed that prestretching of polyampholyte hydrogels accelerates the ion complexation dynamics and fixes the stretched chain conformation thereby producing mechanically anisotropic hydrogels [24].

Because the network chains of high-strength hydrogels are only slightly coiled, even at a modest strain their end-to-end distance approaches their contour length, which limits high prestretch ratios and hence the extent of anisotropic orientation. To overcome this hurdle, we report here a simple one-step method of producing high-strength anisotropic hydrogels. It occurred to us that shape-memory hydrogels would be a good candidate to generate anisotropic hydrogels in a single synthetic step. Such hydrogels generally contain two types of cross-links, namely chemical cross-links (netpoints) determining the permanent shape, and switching segments, e.g., glassy or crystalline domains fixing the temporary shape below their transition temperature T_{trans} [25–32]. Shape-memory hydrogels above T_{trans} exhibit a low modulus of elasticity so that they can be stretched to high elongations whereas upon cooling below T_{trans}, the stretched conformation of the network chains is fixed. This reveals that isotropic hydrogels with a very low stretchability can be made anisotropic providing that they have both netpoints and switching segments in their network structure. Previous work indeed shows appearance of mechanical anisotropy in a commercially available Verflex® thermoset shape-memory polymer induced by a large uniaxial strain [33].

Here, we use semicrystalline physical hydrogels with shape-memory function as the precursor material in generating anisotropic hydrogels. The precursor hydrogels consist of poly(N,N-dimethylacrylamide) (poly (DMAA)) chains interconnected by n-octadecyl acrylate (C18A) segments forming crystalline domains and hydrophobic associations acting as switching segments and netpoints, respectively (Scheme 1) [34–36]. Above the melting temperature T_{m} of C18 crystals which is around 48 °C, the hydrogels exhibit a relatively low and time-dependent modulus due to the finite lifetime of hydrophobic associations holding the chains together, whereas below T_{m}, about half of the associations turns into alkyl crystals thereby producing mechanically strong hydrogels with a high Young's modulus (up to 160 MPa) and tensile fracture stress (up to 6.7 MPa) [32,34,35]. Microstructural and mechanical anisotropy in semicrystalline hydrogels was generated via a single-step procedure as shown in Fig. 1a. We impose a prestretching on the water-swollen isotropic hydrogel samples above T_{m} of their crystalline domains followed by cooling below T_{m} under strain to fix the elongated shape of the gel samples. The prestretch ratio λ_{o} defined as

the ratio of fixed elongated length to the initial length was varied between 1.2 and 8.

As will be seen below, a significant microstructural and mechanical anisotropy was achieved in high strength physical hydrogels, that could be tuned by the magnitude of the prestretch ratio λ_{o}. In the following, we discuss the relation between the microstructure and mechanical properties of anisotropic poly(DMAA-co-C18A) hydrogels consisting of 70 mol % N,N-dimethylacrylamide (DMAA) and 30 mol % C18A together with and without 0.1 mol % non-crystallizable hydrophobic monomer lauryl methacrylate (LM). Small- and wide-angle X-ray scattering measurements and mechanical tests, conducted parallel and perpendicular to the prestretching direction, reveal a critical prestretch ratio λ_{o} at which the hydrogel exhibits the highest microstructural and mechanical anisotropy due to the finite extensibility of the network chains.

2. Experimental

2.1. Preparation of isotropic hydrogels

The synthetic procedure of isotropic hydrogels is the same as that in our previous work (for details, see the Supporting Information) [35,37]. Briefly, DMAA, C18A, and LM monomers were mixed at 45 °C for 10 min to obtain a homogeneous solution. After dissolving 0.1 wt% Irgacure 2959 initiator in this solution, it was transferred into several thin film molds (1 × 5x20 mm) and bulk photopolymerization was conducted at 23 ± 2 °C under UV light at 360 nm for 24 h. The copolymers were then immersed in a large excess of water at a temperature of 70 °C for the first 3 days and 24 ± 1 °C for the following days until attaining a constant gel mass. The gel fraction and the water content of the hydrogels were determined as described before [35,37]. Two hydrogel samples at DMAA/C18A/LM molar ratios of 70/30/0 and 70/29.9/0.1 were prepared which are denoted as 0LM and 0.1LM, respectively (Table 1).

2.2. Preparation of prestretched hydrogels and their characterization

Water-swollen isotropic hydrogel specimens in the form of thin films of about 1 × 5x20 mm in dimensions were used for the preparation of anisotropic hydrogels. Two metal clamps were first placed on both sides of the gel specimen separated by a distance l_{o} in wet condition, as shown in Fig. 2a. The clamps together with the gel specimen were immersed in a water bath at 80 °C for 5 min during which the modulus significantly reduced and the strong gel became a weak gel with a loss factor above 0.1. The specimen was then stretched in water at 80 °C to a clamp-to-clamp distance l_{1} and then immersed in a water bath at 20 °C by fixing the strain. After removing strain, clamp-to-clamp distance l_{1} remained unchanged indicating complete shape-fixing
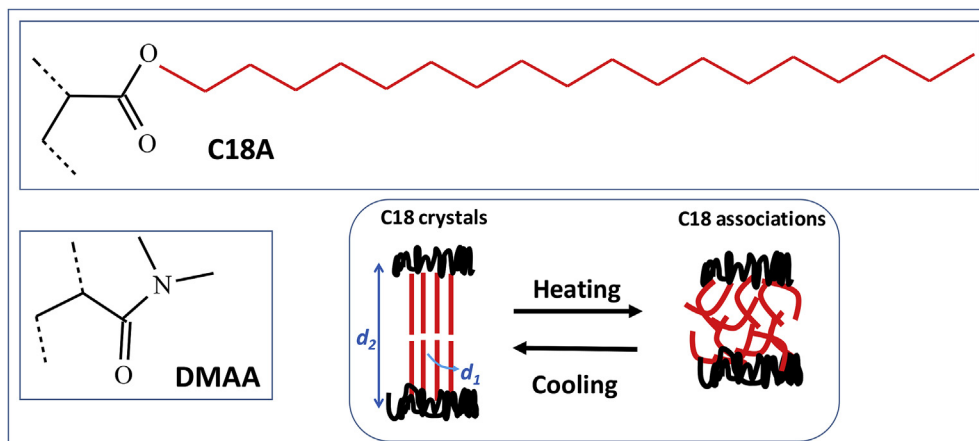
Scheme 1. Structure of DMAA and C18A segments of the hydrogels and a cartoon showing alkyl crystals and hydrophobic associations.[aa] Red lines and curves in the bottom panel represent side alkyl chains of C18A segments in crystals and hydrophobic associations, respectively, while black curves represent the amorphous domains.
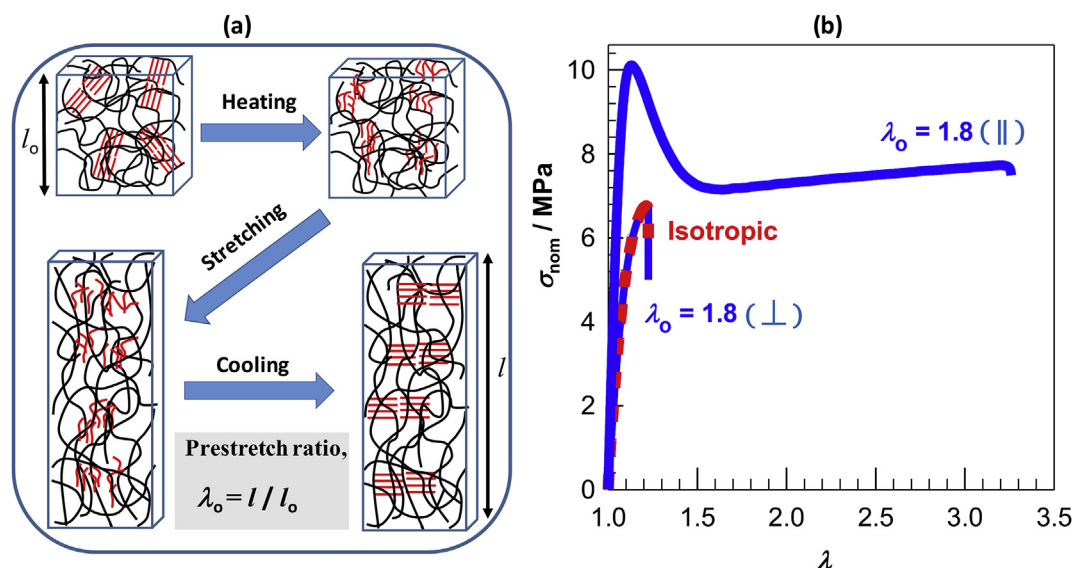
Fig. 1. (a): Cartoon presenting prestretching technique to generate anisotropic hydrogels. Red straight lines and curves are C18 alkyl chains in crystals and associations, respectively. **(b):** Stress-strain curves of isotropic (red dashed curve) and anisotropic 0LM hydrogels at a prestretch ratio $\lambda_o = 1.8$ (blue curves) obtained parallel (∥) and perpendicular to the prestretching direction (⊥). (For interpretation of the references to colour in this figure legend, the reader is referred to the Web version of this article.)

efficiency. The prestretch ratio λ_o calculated as $\lambda_o = l_1/l_0$ was varied between 1.2 and 8. Prestretched hydrogels equilibrium swollen in water were subjected to swelling, rheological, differential scanning calorimetry (DSC), small (SAXS) and wide angle X-ray scattering (WAXS) measurements, and uniaxial tensile tests as described before [35,37], and detailed in Supporting Information section. SAXS and WAXS measurements as well as uniaxial tensile tests were carried out in directions parallel and perpendicular to the prestretching direction.

3. Results and discussion

Semicrystalline hydrogels with an isotropic microstructure were prepared by bulk copolymerization of DMAA with the hydrophobic monomers C18A and LM, followed by swelling of the resulting copolymers in water. The hydrogel denoted by 0LM was prepared at a DMAA/C18A molar ratio of 70/30 without addition of LM, whereas the hydrogel denoted by 0.1LM was prepared in the presence of 0.1 mol % LM, i.e., at a DMAA/C18A/LM molar ratio of 70/29.9/0.1. The characteristics of isotropic 0LM and 0.1LM hydrogels are collected in Table 1. 0LM is a brittle hydrogel and ruptures at a stretch of 20%, whereas 0.1LM is a tough hydrogel sustaining up to 160% stretches. As reported before [35], the toughness improvement upon incorporation of 0.1 mol % LM into the backbone of 0LM hydrogel is due to the formation of more ordered lamellar clusters interconnected by active tie molecules creating an effective energy dissipation mechanism.

To create an anisotropic microstructure, we impose a prestretching on isotropic semicrystalline hydrogel specimens at 80 °C at which they exhibit a low modulus and can easily be stretched. This is illustrated in Fig. 2b where the storage G' and loss moduli G'' of a 0LM hydrogel specimen at 25 and 80 °C are shown as a function of frequency ω. Upon heating from 25 to 80 °C, G' decreases about 3-orders of magnitude and

becomes frequency dependent indicating strong-to-weak gel transition. The stretched chain conformation in the hydrogels at 80 °C was then fixed by cooling to 20 °C as detailed in the experimental section. Using this simple approach, we were able to generate significant mechanical anisotropy in the hydrogels. For instance, the dashed red curve in Fig. 1b presents typical nominal stress (σ_{nom}) – elongation ratio (λ) curve of the brittle 0LM hydrogel specimen with an isotropic microstructure. The blue solid curves in the figure are stress-strain curves of the same hydrogel at $\lambda_o = 1.8$, measured in directions parallel (∥) and perpendicular (⊥) to the prestretching direction. The prestretch ratio of 1.8 creates significant anisotropy as well as brittle-to-ductile transition along the prestretching direction. In the following we discuss the changes in the microstructure and mechanical properties of 0LM and 0.1LM hydrogels depending on the prestretch ratio λ_o which was varied between 1.2 and 8.

3.1. Microstructure of the hydrogels

Fig. 3a shows the equilibrium weight swelling ratio q_w (swollen gel mass/dry mass) of 0LM and 0.1LM hydrogels in water at 23 ± 2 °C plotted against the prestretch ratio λ_o. Prestretching first decreases q_w for both hydrogels up to $\lambda_o = 2.0 \pm 0.1$, as indicated by the dashed vertical line, but then it again increases with a further increase of λ_o. Because the swelling degree of the hydrogels is determined by their cross-link density, the results reveal that prestretching at λ_o below and above 2.0 ± 0.1 has opposite effects on the number of crystals acting as effective cross-links, that is, the crystallinity first increases but then decreases with increasing λ_o. Fig. 3b, c, S1 show DSC scans of 0LM and 0.1 LM hydrogels at various prestretch ratios λ_o. The melting temperature T_m does not change with λ_o and remains at 48.3 ± 0.5 and 47.4 ± 0.5 °C for 0LM and 0.1LM, respectively. However, the degree of

Table 1
Characteristics of isotropic 0LM and 0.1LM hydrogels prior to prestretching.[a]

Code	DMAA mol %	C18A mol %	LM mol %	q_w	T_m °C	x_c %	E/MPa	σ_f/MPa	λ_f	W/MJ m^{-3}
0LM	70	30.0	0	1.35	48	38	71 (4)	6.7 (0.1)	1.2 (0.1)	1.1 (0.1)
0.1LM	70	29.9	0.1	1.36	47	37	74 (7)	5.4 (0.2)	2.6 (0.2)	9.6 (0.4)

[a] q_w = Equilibrium weight swelling ratio in water at 23 ± 2 °C. T_m = Melting temperature. x_c = Degree of crystallinity. E = Young's modulus. σ_f = Fracture stress, λ_f = Fracture strain. W = Energy to break (toughness). Standard deviations are in parentheses while for the q_w 's, they are less than 10%.
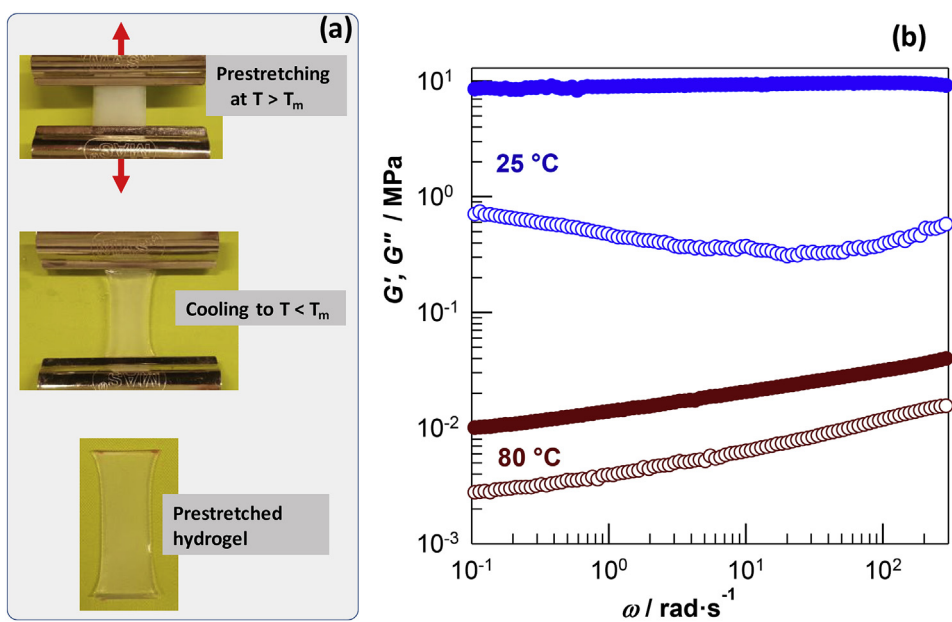
Fig. 2. **(a):** Images showing prestretching of a 0LM hydrogel specimen at 80 °C and then cooling below T_m to obtain a prestretched gel at $\lambda_o = 2$. **(b):** Storage modulus G' (filled symbols) and loss modulus G'' (open symbols) of 0LM hydrogel at 25 and 80 °C. Strain amplitude = 0.1%.
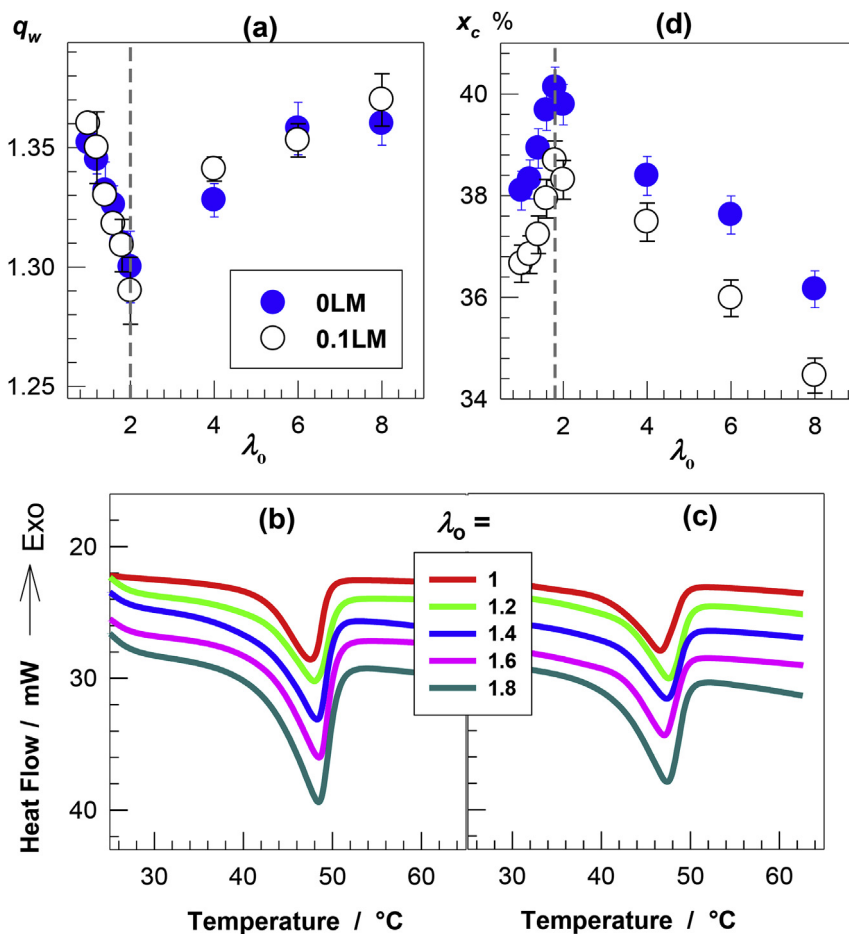
Fig. 3. **(a, d):** The weight swelling ratio q_w at 23 ± 2 °C (a) and the degree of crystallinity x_c (d) of 0LM (filled circles) and 0.1LM hydrogels (open circles) both plotted against the prestretch ratio λ_o. **(b, c):** DSC scans of 0LM (b) and 0.1LM hydrogels (c) at various prestretch ratios λ_o.
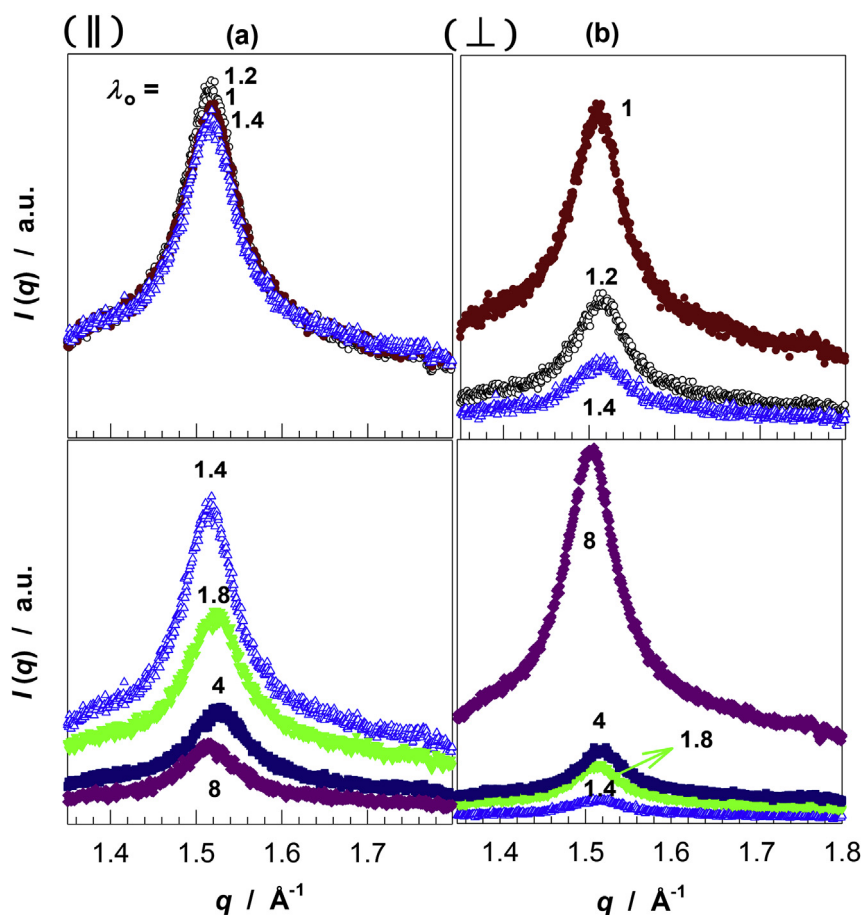
Fig. 4. WAXS profiles of 0LM hydrogels at various prestretch ratios λ_o indicated. The data were recorded in directions parallel (left panel, a) and perpendicular (right panel, b) to the prestretching direction.
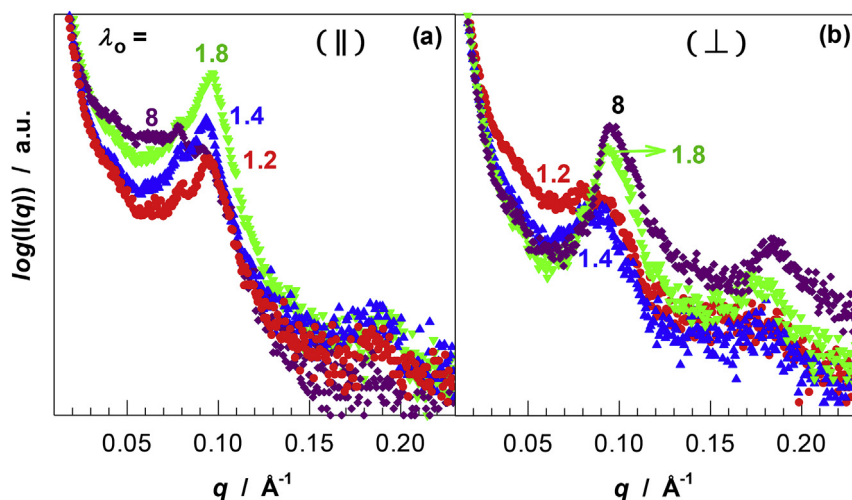
Fig. 5. SAXS profiles of 0LM hydrogels at various prestretch ratios λ_o indicated. The data were recorded in directions parallel (a) and perpendicular (b) to the prestretching direction.

crystallinity x_c calculated from the area under the melting peak depends on the prestretch ratio, as seen in Fig. 3d. In accord with the swelling results, the crystallinity x_c increases with increasing λ_o for $\lambda_o < 1.8 \pm 0.2$ whereas for $\lambda_o > 1.8 \pm 0.2$, it again decreases. Thus, prestretching of the hydrogels in the melt state first facilitates the alignment of alkyl side chains and increases the number of crystalline domains acting as physical cross-links. However, above the threshold value of $\lambda_o = 1.8 \pm 0.2$, the crystallinity again decreases while

swelling ratio increases continuously suggesting disruption of crystalline domains and hence decreasing the cross-link density of the hydrogels.

For a deeper understanding of the microstructure of the hydrogels, WAXS and SAXS measurements were conducted in directions both parallel and perpendicular to the prestretching direction. Fig. 4a and b shows WAXS patterns of 0LM hydrogels at various λ_o from directions parallel (∥) and perpendicular (⊥) to the prestretching direction,

respectively. The data for $\lambda_o \leq 1.4$ and $\lambda_o \geq 1.4$ are shown in the upper and bottom panel, respectively. In both directions, the high intensity peak appears at a scattering vector $q_{max} = 1.52 \pm 0.01\,\text{Å}^{-1}$ corresponding to a lattice spacing d_1 of $4.13 \pm 0.02\,\text{Å}$, which is typical for side-by-side packed alkyl chains (Scheme 1) [29,31,32,38–40]. Thus, the peak position and hence the dimension of the unit cell do not change depending on the prestretch ratio or, on the direction of the measurements.

However, the peak intensity shows a strong prestretch ratio and directional dependencies. Along the prestretching direction (Fig. 4a), the high intensity peak is sharp and the maximum intensity I_{max} is almost constant between $\lambda_o = 1$ and 1.4, but then it decreases and the peak broadens at high λ_o's, as expected due to the decreasing crystallinity at $\lambda_o > 2$ (Fig. 3d). In contrast, I_{max} in perpendicular direction first decreases with λ_o up to $\lambda_o = 1.4$ and then it again increases with increasing λ_o and a sharp high intensity peak appears at the highest prestretch ratio of 8. The constancy of d_1 spacing at $4.13 \pm 0.02\,\text{Å}$ and opposite variations of the peak intensities with λ_o in parallel and perpendicular directions were also observed in 0.1LM hydrogels prepared with 0.1 mol % LM (Fig. S2). The results reveal higher number density of lamellar crystals perpendicularly to the prestretching direction at large prestretch ratios.

SAXS profiles of 0LM hydrogels between $\lambda_o = 1.2$ and 8 are shown in Fig. 5a and b in directions parallel and perpendicular to the prestretching direction, respectively. All hydrogels with and without LM exhibit a high intensity peak at $q_{max} = \sim 0.095\,\text{Å}^{-1}$ corresponding to a lattice spacing d_2 of 6.6 ± 0.1 nm (Fig. 5, S3). This reveals tail-to-tail alignment of octadecyl (C18) side chains perpendicularly to the main chain [29,31], as illustrated in Scheme 1. Because the fully extended C18 chain length is 2.43 nm [35], this also reveals that the thickness of amorphous poly(DMAA) domains between alkyl crystals is around 1.7 nm. The peak intensity in parallel direction increases with prestretch ratio up to 1.8 while in perpendicular direction, broad peaks with lower intensities were recorded. The result thus reveals that the lamellar crystals align along the prestretching direction while those in perpendicular direction become more disordered. Moreover, remarkable is the almost structureless SAXS pattern at $\lambda_o = 8$ in parallel direction while the appearance of the highest intensity peak in perpendicular direction which we attribute formation of ordered crystallites vertical to the prestretching direction. Thus we may conclude that randomly oriented lamellar stacks in the hydrogels align along the stretching direction at $\lambda_o \leq 1.8$ while a change in the alignment from parallel to perpendicular stretching direction appears at high stretch ratios.

3.2. Correlation between mechanical properties and microstructure of the hydrogels

Fig. 6a shows uniaxial tensile stress-strain curves of 0LM hydrogels at various prestretch ratios λ_o between 1.2 and 8. The curves for the reference hydrogel without prestretching ($\lambda_o = 1$) are also shown by the dashed curves. The tests were carried out parallel ($\parallel$, left panel) and perpendicular to the prestretching direction ($\perp$, right panel). Except the reference non-prestretched hydrogel, all hydrogels exhibit anisotropic mechanical properties. Moreover, in accord with the microstructural changes in the hydrogels, their mechanical performance shows different prestretch ratio dependences at below and above 1.8. For the sake of clarity, the data for $\lambda_o \leq 1.8$ and $\lambda_o \geq 1.8$ are shown in the upper and bottom panels of Fig. 6a, respectively. Two distinct regimes can be seen from the plots:

(ı) $\lambda_o \leq 1.8$: The brittle reference hydrogel becomes tough along the prestretching direction while it remains brittle in perpendicular direction. The brittle-to-ductile transition could be induced even at the lowest prestretch ratio λ_o of 1.2; both the yield stress and the fracture strain increase continuously with λ_o.

(ıı) $\lambda_o \geq 1.8$: The yield stress and fracture strain start to decrease with increasing λ_o along the prestretching direction and at the highest prestretch ratio of 8, the hydrogel fractures without yielding. Simultaneously, strain hardening behavior appears and the stress continuously increases up to the fracture point. In perpendicular direction, hydrogel starts to toughen with increasing λ_o with the appearance of yielding behavior at $\lambda_o = 4$, above which both the yield stress and fracture strain continuously increase with λ_o up to 8.

The opposite effect of λ_o at below and above 1.8 on the mechanical properties is also illustrated in Fig. 6b where the Young's modulus E, yield stress σ_y, fracture strain λ_f, and the energy to break W (toughness) of the hydrogels measured at parallel (filled symbols) and perpendicular directions (open symbols) are plotted against λ_o. General trend at below and above $\lambda_o = 1.8$ is the increase of the modulus, toughness, yield stress, and fracture strain with increasing λ_o in parallel and perpendicular directions, respectively. The maximum degree of mechanical anisotropy in the hydrogels appears at the prestretch ratio of 1.8, as indicated by vertical gray lines in the figures. For instance, the hydrogel at this prestretch ratio sustains 220 and 25% elongations and exhibits Young's moduli of 161 ± 14 and 76 ± 7 MPa, toughness of 16 ± 1 and 1.3 ± 0.1 MJ m^{-3} along and vertical to the prestretching direction, respectively. The extent of mechanical anisotropy is generally given by the ratio of a mechanical property such as the modulus measured in directions parallel to perpendicular to the orientation of the material [3]. At $\lambda_o = 1.8$, the anisotropy with respect to the modulus and toughness attains a maximum value of 2.1 ± 0.2 and 12 ± 1, respectively (Fig. S4). Interestingly, the modulus anisotropy at $\lambda_o = 8$ is 0.56, i.e., 1/1.8, indicating the existence of the same extent of modulus anisotropy in favor of perpendicular direction.

Similar results were also observed for 0.1LM hydrogels prepared with 0.1 mol% LM. Fig. 7a and b shows stress-strain curves and mechanical parameters of 0.1LM hydrogels at various prestretch ratios. The non-prestretched 0.1LM hydrogel is already tough and exhibits isotropic mechanical properties. Its stretchability and toughness further increase along the prestretching direction while it becomes brittle in perpendicular direction. Interesting is the appearance of tough-to-brittle transition in vertical direction by imposing the lowest prestretch ratio of 1.2. Thus, brittle-to-ductile and ductile-to-brittle transitions in 0LM and 0.1LM hydrogels could be induced in parallel or perpendicular directions, respectively, at low prestretch ratios. The results thus reveal that the orientation of the alkyl crystals in a given direction leads to directional toughness improvement in semicrystalline hydrogels. This finding is in accord with our previous report showing that incorporation of 0.1–0.4 mol % LM segments into the backbone of semicrystalline hydrogels generate more ordered lamellar clusters with a layered structure, which was accompanied by a brittle-to-ductile transition [35]. In the present work, ordered lamellar clusters were generated by prestretching of the network chains instead of LM addition so that a directional improvement in the mechanical performance of the hydrogels was observed.

As schematically illustrated in Fig. 8a, lamellar clusters (enclosed in rectangles) are composed of several lamellar crystals separated by amorphous domains. The tie molecules bridging the clusters have an important role in the mechanical properties of semicrystalline polymers [41–47]. Prestretching the hydrogel above T_m followed by cooling below T_m creates aligned lamellar crystals to the prestretching direction (Fig. 8a). Moreover, because the thickness L of the lamellar clusters is in the range of the end-to-end distance of the polymer chains in unperturbed state [41,42], this thickness will increase to $\lambda_o L$ in prestretched hydrogels producing thicker lamellar clusters. Stretching the hydrogel parallel to the prestretching direction produces a stress on the lamellar clusters through the tie molecules leading to their bending and finally fragmentation at the yield point (Fig. 8b). Because of the increased thickness of lamellar cluster with increasing prestretch ratio λ_o,
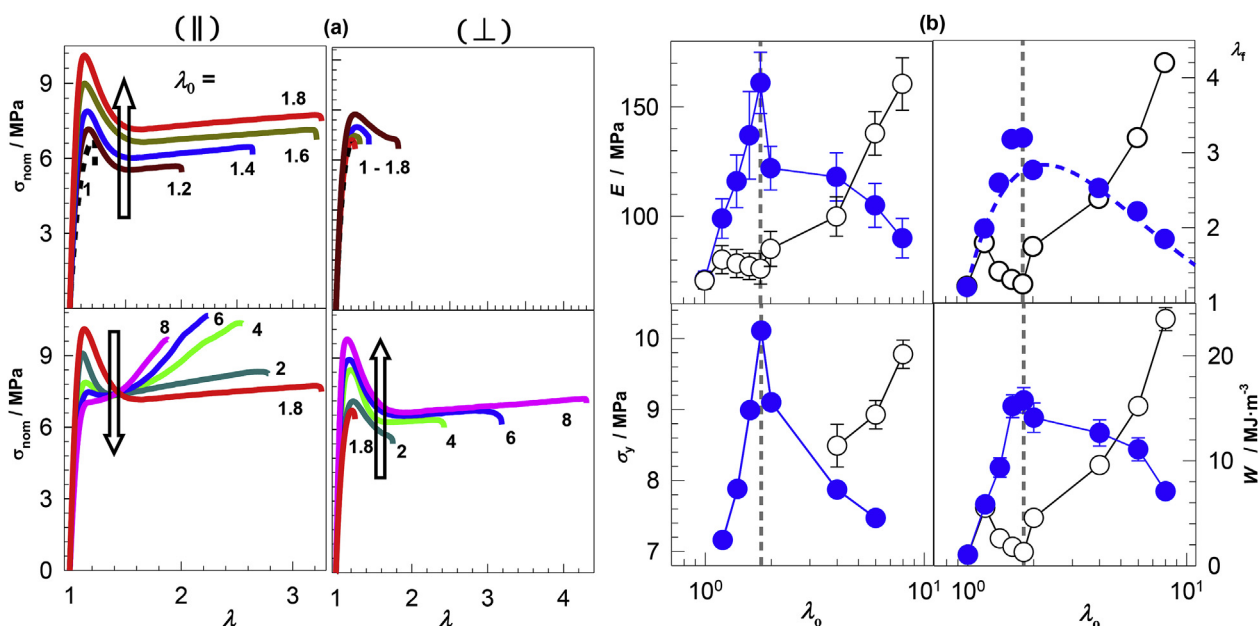
Fig. 6. (a): Stress-strain curves of 0LM hydrogels at various stretch ratios λ_o indicated. The measurements were conducted in directions parallel (∥) and perpendicular (⊥) to the prestretching. Strain rate: 5 min^{-1}. **(b):** Prestretch ratio dependences of Young's modulus E, yield stress σ_y, fracture strain λ_f, and energy to break (toughness) W of the hydrogels measured along parallel (filled symbols) and perpendicular to the prestretching direction (open symbols). The vertical dashed line represents the data at $\lambda_o = 1.8$. The dashed curve was calculated using eq (3) for $\lambda_{f,n} = 1.2 \pm 0.1$.

a higher stress and a lower deflection will be required for fragmentation of thicker lamellar clusters. Indeed, as shown in Figs. 6b and 7b, S5, the yield stress σ_y increases whereas the yield strain λ_y decreases with increasing λ_o up to 1.8 for both 0LM and 0.1LM hydrogels. On the other hand, stretching the hydrogel perpendicular to the prestretching direction does not produce a significant stress on the lamellar clusters, as illustrated in Fig. 8c. Tie molecules and amorphous domains of the clusters are pulled away from the clusters leading to the formation of thinner and closer clusters. Thus, the hydrogels exhibit a low modulus and toughness when measured perpendicular to the prestretching direction. Fragmentation of the thin clusters and appearance of yield

point thus require high prestretch ratios at which the tie molecules are highly stretched.

Fragmentation of lamellar clusters results in dissipation of energy while being stretched so that resistance to crack propagation is observed. Because the clusters are irreversibly broken at the yield point, this suggests that the yielding behavior will disappear if a hydrogel specimen is subjected to second stretching. This was indeed observed. Fig. 9a shows nominal stress σ_{nom} vs strain ε (= λ - 1) plots from five successive tensile cycles conducted parallel to the prestretching direction on 0LM hydrogel at $\lambda_o = 1.8$. The tests were carried out up to a maximum strain of 110% where up and down arrows in the figure
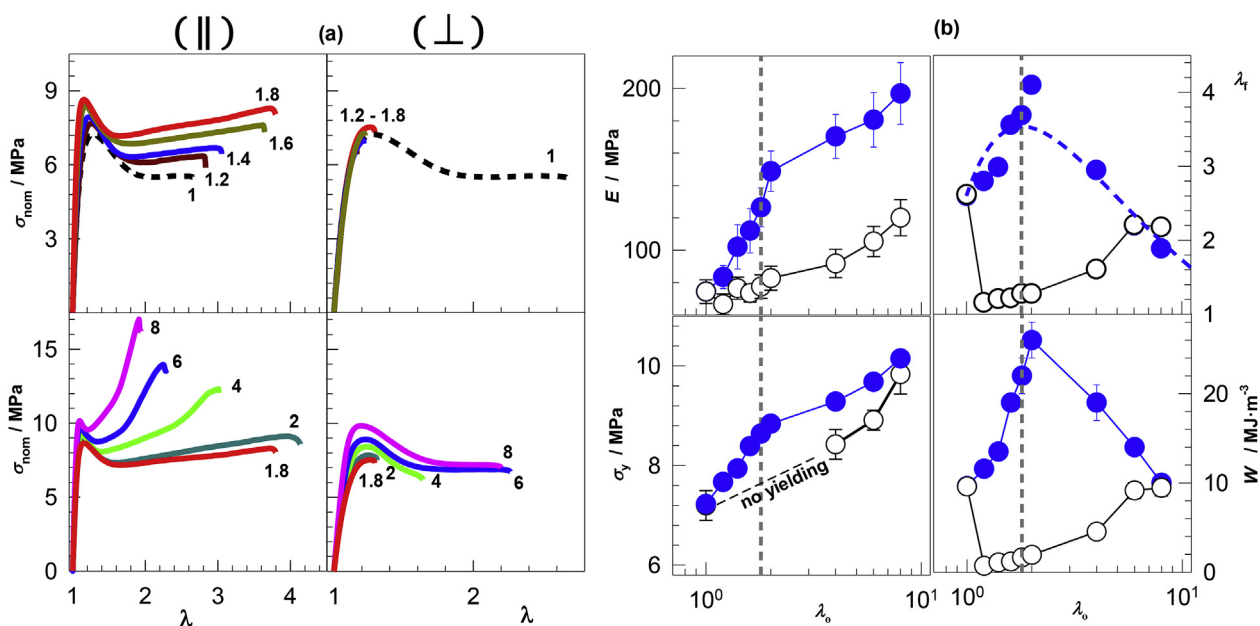
Fig. 7. (a): Stress-strain curves of 0.1LM hydrogels at various stretch ratios λ_o measured in parallel (∥) and perpendicular to the prestretching directions (⊥). Strain rate: 5 min^{-1}. (b): E, σ_y, λ_f, and W of the hydrogels along parallel (filled symbols) and perpendicular directions (open symbols) plotted against λ_o. The dashed curve was calculated using eq (3) for $\lambda_{f,n} = 2.6 \pm 0.2$.
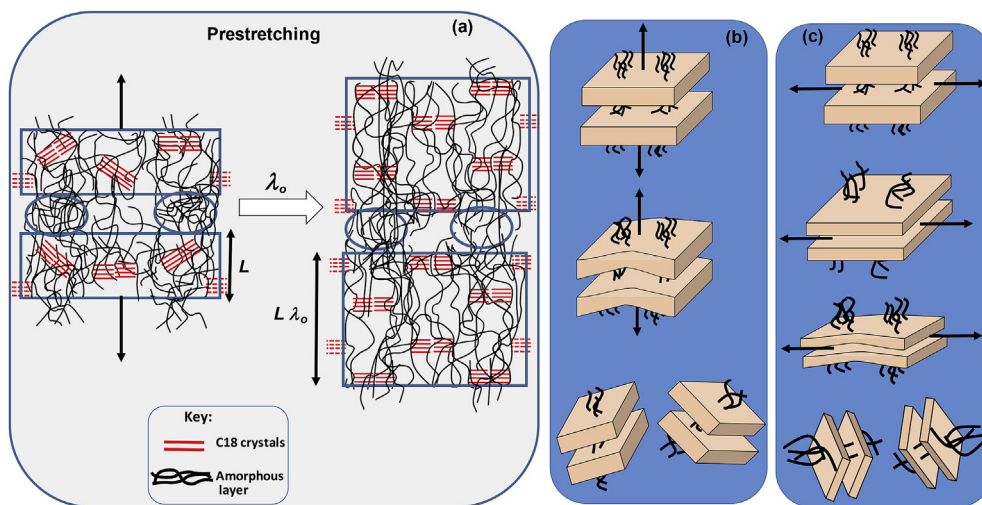
Fig. 8. (a): Cartoon showing lamellar clusters interconnected by active tie molecules before and after prestretching. Lamellar clusters and tie molecules are enclosed in rectangles and circles, respectively. **(b, c):** Stretching lamellar clusters parallel (b) and perpendicular to the prestretching direction.

indicate loading and unloading steps, respectively. It is seen that the first loading significantly deviates from the following loadings and produces 4- to 5-fold larger hysteresis energy as compared to the following cycles (Fig. S6). The modulus of the first loading curve is around 100-fold larger as compared to that of the following loadings revealing the occurrence of an irreversible damage in the hydrogel due to the broken lamellar clusters at the yield point. Similar results were also obtained at larger prestretch ratios λ_o when the tests are conducted perpendicular to the prestretching direction (Fig. S6).

After the yield point, that is, after fragmentation of lamellar clusters, tie molecules are stretched out from the fragmented clusters until they can be pulled out no further without rupture. As seen in Figs. 6b and 7b, the stretch at rupture of tie molecules, that is the fracture strain λ_f of both hydrogels along the prestretching direction exhibits a maximum at around $\lambda_o = 1.8$. We have to mention that because tensile tests on the hydrogels start from the value $\lambda = \lambda_o$ instead of $\lambda = 1$, the true fracture strain $\lambda_{f,true}$ with respect to the as-prepared state is the product λ_f and λ_o, which is larger than the nominal value λ_f. Let $\lambda_{f,n}$ be the fracture strain of non-prestretched hydrogel, the excess chain extension at break $\Delta\lambda$ of prestretched hydrogels over $\lambda_{f,n}$ can thus be given by:

$$\Delta\lambda = \lambda_{f,true} - \lambda_{f,n} = \lambda_f \lambda_o - \lambda_{f,n} \qquad (1)$$

In Fig. 9b, the excess chain extension $\Delta\lambda$ for 0LM and 0.1LM hydrogels along the prestretching direction is plotted in a semi-logarithmic scale against the prestretch ratio λ_o. The best fitting curve to the data shown in the figure indicates that the excess chain extension at break is linear in $ln(\lambda_o)$, given by the equation,

$$\Delta\lambda = n \ln(\lambda_o) \qquad (2)$$

where n is a constant and equal to 6.4 $\pm$ 0.1. By substituting of eq (1) into eq (2), we obtain:

$$\lambda_f = (\lambda_o)^{-1} [\lambda_{f,n} + n \ln(\lambda_o)] \qquad (3)$$

presenting the prestretch ratio dependence of the fracture strain of the hydrogels (dashed curves in Figs. 6b and 7b). Taking derivative of λ_f with respect to λ_o and equating to zero, one may calculate λ_f and λ_o at the maximum point in λ_f vs λ_o curves as:

$$\lambda_{f,max} = \frac{n}{\lambda_o} \qquad or \quad \lambda_{f,true,max} = n \qquad (3a)$$

$$\lambda_{o,max} = \exp\left(1 - \frac{\lambda_{f,n}}{n}\right) \qquad (3b)$$

Eq (3a) reveals that the constant $n = 6.4 \pm 0.1$ is the maximum extension ratio ($\lambda_{f,true,max}$) of tie molecules with respect to the as-prepared state, above which they rupture. Because $\lambda_{f,n} = 1.2 \pm 0.1$ and 2.6 $\pm$ 0.2 for 0LM and 0.1LM hydrogels, respectively, eq (3b) reveals that the maximum extension ratio n of tie molecules is reached at $\lambda_{o,max} = 2.0 \pm 0.2$ for the present hydrogels, which is close to the critical prestretch ratio of around 1.8. Thus, the period $\lambda_o < 1.8$ corresponds to the flexible regime where the tie molecules between fragmented clusters are coiled so that λ_f increases with increasing λ_o. However, at larger values of λ_o, the maximum extension n of tie molecules is reached earlier, that is, at a lower strain as λ_o is increased. The results also reveal that the limited extensibility of tie molecules above
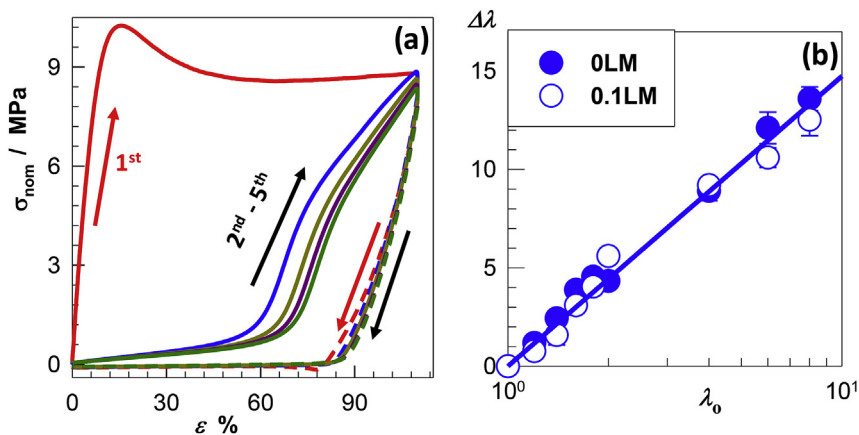
Fig. 9. (a). σ_{nom} vs strain ε (= λ - l) plots from five successive tensile cycles up to a maximum strain of 110% conducted parallel to the prestretching direction on 0LM hydrogel at $\lambda_o = 1.8$. Up and down arrows indicate loading and unloading steps, respectively. Strain rate: 5 min^{-1}. **(b):** Excess chain extension at break $\Delta\lambda$ of 0LM and 0.1LM hydrogels plotted against logarithm of the prestretch ratio λ_o. The line is the best-fitting curve to the experimental data with a slope 6.4 $\pm$ 01.

$\lambda_o = 4$ is responsible for the appearance of strain hardening behavior in hydrogels (Figs. 6 and 7).

4. Conclusions

We present a simple technique for production of mechanically strong physical hydrogels with anisotropic properties. Semicrystalline hydrogels composed of poly(DMAA) chains interconnected by C18 crystals and associations were used as the precursor material in producing anisotropic hydrogels. Microstructural and mechanical anisotropy in the hydrogels was generated by imposing a prestretching on the water-swollen isotropic hydrogel samples in the melt state followed by cooling below T_m to fix the elongated shape of the samples. Swelling tests and DSC measurements reveal that prestretching first facilitates the alignment of alkyl side chains and increases the number of crystalline domains acting as physical cross-links. However, above the threshold value of $\lambda_o = 1.8 \pm 0.2$, the crystallinity again decreases while swelling ratio increases continuously suggesting disruption of crystalline domains and hence decreasing the cross-link density of the hydrogels. SAXS profiles of the hydrogels indicate that randomly oriented lamellar stacks in the hydrogels align along the stretching direction at $\lambda_o \leq 1.8$ while a change in the alignment from parallel to perpendicular stretching direction appears at high stretch ratios. In accord with the SAXS results, the mechanical performance of the hydrogels shows different prestretch ratio dependences at below and above 1.8. At $\lambda_o \leq 1.8$, the brittle isotropic hydrogel becomes tough along the prestretching direction with increasing λ_o while it remains brittle in perpendicular direction. However, at $\lambda_o \geq 1.8$, the mechanical performance of the hydrogel deteriorates along the prestretching direction while in perpendicular direction, hydrogel starts to toughen with increasing λ_o. At the critical prestretch ratio $\lambda_o = 1.8$, the hydrogel exhibits the highest microstructural and mechanical anisotropy due to the finite extensibility of the network chains.

Acknowledgments

Appendix A. Supplementary data

Supplementary data related to this article can be found at https://doi.org/10.1016/j.polymer.2018.07.077.

References

[1] P. Calvert, Hydrogels for soft machines, Adv. Mater. 21 (2009) 743–756.
[2] C. Creton, 50th Anniversary perspective: networks and gels: soft but dynamic and tough, Macromolecules 50 (2017) 8297–8316.
[3] K. Sano, Y. Ishida, T. Aida, Synthesis of anisotropic hydrogels and their applications, Angew. Chem. Int. Ed. 57 (2018) 2–14.
[4] Q. Lu, S. Bai, Z. Ding, H. Guo, Z. Shao, H. Zhu, D.L. Kaplan, Hydrogel assembly with hierarchical alignment by balancing electrostatic forces, Adv. Mater. Interfaces 3 (2016) 1500687.
[5] X.Y. Lin, Z.J. Wang, P. Pan, Z.L. Wu, Q. Zhenga, Monodomain hydrogels prepared by shear-induced orientation and subsequent gelation, RSC Adv. 6 (2016) 95239–95245.
[6] Z. Zhu, Y. Li, H. Xu, X. Peng, Y.-N. Chen, C. Shang, Q. Zhang, J. Liu, H. Wang, Tough and thermosensitive poly(N-isopropylacrylamide)/graphene oxide hydrogels with macroscopically oriented liquid crystalline structures, ACS Appl. Mater. Interfaces 8 (2016) 15637–15644.
[7] M. Liu, Y. Ishida, Y. Ebina, T. Sasaki, T. Hikima, M. Takata, T. Aida, An anisotropic hydrogel with electrostatic repulsion between cofacially aligned nanosheets, Nature 517 (2015) 68–72.
[8] K. Kaneda, K. Uematsu, H. Masunaga, Y. Tominaga, K. Shigehara, K. Shikinaka, Flow-orientation of internal structure and anisotropic properties on hydrogels consisted of imogolite hollow nanofibers, Seni Gakkai Shi 70 (2014) 137–144.
[9] E. Paineau, I. Dozov, I. Bihannic, C. Baravian, M.-E.M. Krapf, A.-M. Philippe, S. Rouzière, L.J. Michot, P. Davidson, Tailoring highly oriented and micropatterned clay/polymer nanocomposites by applying an a.c. electric field, ACS Appl. Mater. Interfaces 4 (2012) 4296–4301.
[10] S. Isabettini, S. Stucki, S. Massabni, M.E. Baumgartner, P.Q. Reckey, J. Kohlbrecher, T. Ishikawa, E.J. Windhab, P. Fischer, S. Kuster, Development of smart optical gels with highly magnetically responsive bicelles, ACS Appl. Mater. Interfaces 10 (2018) 8926–8936.
[11] B. Yetiskin, O. Okay, High-strength silk fibroin scaffolds with anisotropic mechanical properties, Polymer 112 (2017) 61–70.
[12] L.E. Millon, H. Mohammadi, W.K. Wan, Anisotropic polyvinyl alcohol hydrogel for cardiovascular applications, J. Biomed. Mater. Res. B Appl. Biomater. 79 (2006) 305–311.
[13] W. Wan, A.D. Bannerman, L. Yang, H. Mak, Poly(vinyl alcohol) cryogels for biomedical applications, Adv. Polym. Sci. 263 (2014) 283–321.
[14] T. Kaneko, D. Ogomi, R. Mitsugi, T. Serizawa, M. Akashi, Mechanically drawn hydrogels uniaxially orient hydroxyapatite crystals and cell extension, Chem. Mater. 16 (2004) 5596–5601.
[15] S. Choi, J. Kim, Designed fabrication of super-stiff, anisotropic hybrid hydrogels via linear remodeling of polymer networks and subsequent crosslinking, J. Mater. Chem. B 3 (2015) 1479–1483.
[16] P. Lin, T. Zhang, X. Wang, B. Yu, F. Zhou, Freezing molecular orientation under stretch for high mechanical strength but anisotropic hydrogels, Small 12 (2016) 4386–4392.
[17] S.H. Kim, S.-K. Im, S.-J. Oh, S. Jeong, E.-S. Yoon, C.J. Lee, N. Choi, E.-M. Hur, Anisotropically organized three-dimensional culture platform for reconstruction of a hippocampal neural network, Nat. Commun. 8 (2017) 14346.
[18] D. Ye, Q. Cheng, Q. Zhang, Y. Wang, C. Chang, L. Li, H. Peng, L. Zhang, Deformation drives alignment of nanofibers in framework for inducing anisotropic cellulose hydrogels with high toughness, ACS Appl. Mater. Interfaces 9 (2017) 43154–43162.
[19] X. He, Y. Oishi, A. Takahara, K. Kajiyama, Higher order structure and thermo-responsive properties of polymeric gel with crystalline side chains, Polym. J. 28 (1996) 452–457.
[20] W. Yang, H. Furukawa, J.P. Gong, Highly extensible double-network gels with self-assembling anisotropic structure, Adv. Mater. 20 (2008) 4499–4503.
[21] Z.L. Wu, T. Kurokawa, D. Sawada, J. Hu, H. Furukawa, J.P. Gong, Anisotropic hydrogel from complexation-driven reorientation of semirigid polyanion at Ca2+ diffusion flux front, Macromolecules 44 (2011) 3535–3541.
[22] Z.L. Wu, D. Sawada, T. Kurokawa, A. Kakugo, W. Yang, H. Furukawa, J.P. Gong, Strain-induced molecular reorientation and birefringence reversal of a robust, anisotropic double-network hydrogel, Macromolecules 44 (2011) 3542–3547.
[23] F. Khan, D. Walsh, A.J. Patil, A.W. Perriman, S. Mann, Self-organized structural hierarchy in mixed polysaccharide sponges, Soft Matter 5 (2009) 3081–3085.
[24] K. Cui, T.L. Sun, T. Kurokaw, T. Nakajimai, T. Nonoyama, L. Chenc, J.P. Gong, Stretching-induced ion complexion in physical polyampholyte hydrogels, Soft Matter 12 (2016) 8833–8840.
[25] A. Lendlein, S. Kelch, Shape-memory polymers, Angew. Chem. Int. Ed. 41 (2002) 2034–2057.
[26] C. Liu, H. Qin, P.T. Mather, Review of progress in shape memory polymers, J. Mater. Chem. 17 (2007) 1543–1558.
[27] T. Xie, Tunable polymer multi-shape memory effect, Nature 464 (2010) 267–270.
[28] Q. Zhao, H.J. Qi, T. Xie, Recent progress in shape memory polymer: new behavior, enabling materials, and mechanistic understanding, Prog. Polym. Sci. 49–50 (2015) 79–120.
[29] A. Matsuda, J. Sato, H. Yasunaga, Y. Osada, Order-disorder transition of a hydrogel containing an n-alkyl acrylate, Macromolecules 27 (1994) 7695–7698.
[30] Y. Osada, A. Matsuda, Shape memory in hydrogels, Nature 376 (1995) 219.
[31] Y. Tanaka, Y. Kagami, A. Matsuda, Y. Osada, Thermoreversible transition of tensile modulus of hydrogel with ordered aggregates, Macromolecules 28 (1995) 2574–2576.
[32] C. Bilici, O. Okay, Shape memory hydrogels via micellar copolymerization of acrylic acid and n-octadecyl acrylate in aqueous media, Macromolecules 46 (2013) 3125–3131.
[33] R. Beblo, L.M. Weiland, Strain induced anisotropic properties of shape memory polymer, Smart Mater. Struct. 17 (2008) 055021 (7pp).
[34] C. Bilici, V. Can, U. Nöchel, M. Behl, A. Lendlein, O. Okay, Melt-processable shape-memory hydrogels with self-healing ability of high mechanical strength, Macromolecules 49 (2016) 7442–7449.
[35] C. Bilici, S. Ide, O. Okay, Yielding behavior of tough semicrystalline hydrogels, Macromolecules 50 (2017) 3647–3654.
[36] D. Wei, J. Yang, L. Zhu, F. Chen, Z. Tang, G. Qin, Q. Chen, Semicrystalline hydrophobically associated hydrogels with integrated high performances, ACS Appl. Mater. Interfaces 10 (2018) 2946–2956.
[37] B. Kurt, U. Gulyuz, D.D. Demir, O. Okay, High-strength semi-crystalline hydrogels with self-healing and shape memory functions, Eur. Polym. J. 81 (2016) 12–23.
[38] N.A. Plate, V.P. Shibaev, Comb-like polymers. Structure and properties, Macromol. Rev. 8 (1974) 117–253.
[39] T. Miyazaki, K. Yamaoka, J.P. Gong, Y. Osada, Hydrogels with crystalline or liquid crystalline structure, Macromol. Rapid Commun. 23 (2002) 447–455.
[40] M. Uchida, M. Kurosawa, Y. Osada, Swelling process and order-disorder transition of hydrogel containing hydrophobic ionizable groups, Macromolecules 28 (1995) 4583–4586.
[41] K.-H. Nitta, M. Takayanagi, Role of tie molecules in the yielding deformation of isotactic polypropylene, J. Polym. Sci. B Polym. Phys. 37 (1999) 357–368.
[42] K.-H. Nitta, M. Takayanagi, Tensile yield of isotactic polypropylene in terms of a lamellar-cluster model, J. Polym. Sci. B Polym. Phys. 38 (2000) 1037–1044.
[43] K.-H. Nitta, M. Takayanagi, Novel proposal of lamellar clustering process for elucidation of tensile yield behavior of linear polyethylenes, J. Macromol. Sci. B. Phys.

B42 (2003) 107–126.

[44] R. Gao, M. Kuriyagawa, K.-H. Nitta, X. He, B. Liu, Structural interpretation of Eyring activation parameters for tensile yielding behavior of isotactic polypropylene solids, J. Macromol. Sci. B. Phys. B54 (2015) 1196–1210.

[45] S. Humbert, O. Lame, J.-M. Chenal, C. Rochas, G. Vigier, Small strain behavior of polyethylene: in situ SAXS measurements, J. Polym. Sci. B Polym. Phys. 48 (2010) 1535–1542.

[46] Z. Spitalsky, T. Bleha, P. Cifra, Energy elasticity of tie molecules in semicrystalline polymers, Macromol. Theory Simul. 11 (2002) 513–524.

[47] H. Guo, Y. Zhang, F. Xue, Z. Cai, Y. Shang, J. Li, Y. Chen, Z. Wu, S. Jiang, In-situ synchrotron SAXS and WAXS investigations on deformation and α–β transformation of uniaxial stretched poly(vinylidene fluoride), CrystEngComm 15 (2013) 1597–1606.